Soft Matter

PAPER

View Article Online
View Journal | View Issue

Cite this: *Soft Matter*, 2014, **10**, 9695

Redox control of GPx catalytic activity through mediating self-assembly of Fmoc-phenylalanine selenide into switchable supramolecular architectures†

Zupeng Huang,[a] Quan Luo,[a] Shuwen Guan,[b] Jianxiong Gao,[c] Yongguo Wang,[a] Bo Zhang,[a] Liang Wang,[a] Jiayun Xu,[a] Zeyuan Dong*[a] and Junqiu Liu*[a]

Received 10th September 2014
Accepted 11th October 2014

DOI: 10.1039/c4sm02030h

www.rsc.org/softmatter

Artificial enzymes capable of achieving tunable catalytic activity through stimuli control of enzymatic structure transition are of significance in biosensor and biomedicine research. Herein we report a novel smart glutathione peroxidise (GPx) mimic with modulatory catalytic activity based on redox-induced supramolecular self-assembly. First, an amphiphilic Fmoc-phenylalanine-based selenide was designed and synthesized, which can self-assemble into nanospheres (NSs) in aqueous solution. The NSs demonstrate extremely low GPx activity. Upon the oxidation of hydroperoxides (ROOH), the selenide can be quickly transformed into the selenoxide form. The change of the molecular structure induces complete morphology transition of the self-assemblies from NSs to nanotubes (NTs), resulting in great enhancement in the GPx catalytic activity. Under the reduction of GSH, the selenoxide can be further reversibly reduced back into the selenide; therefore the reversible switch between the NSs and NTs can be successfully accomplished. The relationship between the catalytic activity and enzymatic structure was also investigated. The dual response nature makes this mimic play roles of both a sensor and a GPx enzyme at the same time, which can auto-detect the signal of ROOH and then auto-change its activity to achieve quick or slow/no scavenging of ROOH. The dynamic balance of ROOH is vital in organisms, in which an appropriate amount of ROOH does benefit to the metabolism, whereas surplus ROOH can cause oxidative damage of the cell instead and this smart mimic is of remarkable significance. We expect that such a mimic can be developed into an effective antioxidant drug and provide a new platform for the construction of intelligent artificial enzymes with multiple desirable properties.

Introduction

Reactive oxygen species (ROS), including hydrogen peroxide (H_2O_2) and organic hydroperoxides (ROOH), are created during the organism's metabolism.[1] In natural physiological conditions, they are friendly to the body and play important roles in signalling and maintaining homeostasis of cell.[1] Normally, there is a balance between the creation and decomposition of ROS. However, once the balance is broken, the surplus ROS will cause oxidative damage to the cell, resulting in many relevant diseases such as cataract, Keshan disease, cardiovascular disease and neuronal apoptosis.[2,3] In general, the surplus ROS can be effectively scavenged by two defensive systems: enzymatic and non-enzymatic systems. Among the enzymatic oxidative system, glutathione peroxidases (GPxs) play pivotal roles, which can effectively catalyze the decomposition of ROOH by using GSH as reducing substrate.[2–6] Although natural GPxs can be used as excellent antioxidant drugs, their drawbacks, such as high price, easy deactivation, difficult heterogeneous expression and proteolytic digestion, limit the pharmacological application. Therefore, design and synthesis of new artificial GPx mimics becomes considerably meaningful.

In the past several decades, considerable efforts have been made to simulate the antioxidant efficiency and to reveal the catalytic mechanism of GPxs. Up to now, a great amount of successful artificial GPx mimics have been developed, including selenium- or tellurium-containing small organic compounds,[7–11] macromolecule-based models[12–15] and supramolecular scaffold-based nanoenzymes.[16–18] As examples, Mugesh and co-workers synthesized a number of seleno/telluro-compounds to investigate the relationship between the GPx activity and the microenvironment of the catalytic moieties.[10]

[a]State Key Laboratory of Supramolecular Structure and Materials, College of Chemistry, Jilin University, Changchun 130012, People's Republic of China. E-mail: junqiuliu@jlu.edu.cn; zdong@jlu.edu.cn; Fax: +86-431-85193421

[b]School of Life Science, Jilin University, Changchun 130012, People's Republic of China

[c]State Key Laboratory of Inorganic Synthesis and Preparative Chemistry, College of Chemistry, Jilin University, Changchun 130012, People's Republic of China

† Electronic supplementary information (ESI) available. See DOI: 10.1039/c4sm02030h

Luo *et al.* introduced diselenium to the surface of β-cyclodextrin and prepared 2,2-diselenobis(2-deoxy-β-cyclodextrin), which demonstrates that the binding of the substrate from the hydrophobic cavity of cyclodextrin can effectively improve the activity.[13] In one of our previous work, by incorporating tellurocysteine into glutathione transferase, an ideal mimic that combined a native binding site of GSH with a catalytic residue tellurocysteine (TeCys) was generated, exhibiting remarkable GPx activity that rivals that of the natural GPxs.[15]

Given that only the appropriate amount of ROS benefits the human body, it should not be cleared out completely. Therefore, the fabrication of smart GPx mimics with controllable catalytic activity will have high advantages. Inspired by the development of stimulus-responsive materials and devices, which can be regulated by some extrinsic conditions, such as pH, temperature, sonication, light irradiation and ion strength electric potential, our group successfully constructed some extrinsic stimuli controlled smart GPx mimics with tunable catalytic activity in recent years, for example, temperature-responsive polymer mimics[19–21] and Ca^{2+} responsive protein mimic. These smart mimics can achieve stimulus-controlled catalytic activity. However, the introduction of extrinsic stimuli may cause other problems such as physiological instability and organism rejection. Moreover, if the mimics are applied to organisms, introducing the extrinsic stimuli into body is still a big challenge. Taking into account these weaknesses, we wondered whether it was possible to design a new GPx mimic with controllable activity upon internal triggers, *i.e.* ROOH and GSH. The desirable GPx mimic should meet the following requirements: when the ROOH are overproduced, it exhibits high catalytic efficiency to quickly scavenge ROOH; when the ROOH are reduced, it exhibits relatively low or even no catalytic activity.

In natural GPxs and their mimics, selenium (Se) is used as the catalytic center to catalyze the reactions. However, the utilization of Se is more than that. Se is also an excellent redox-sensitive motif that has been applied to fabricate smart materials.[22–25] Zhang and Xu developed a series of Se-containing polymers with redox-controllable self-assembly properties.[22–24] Yang and Xu introduced Se into histidine-containing peptide.[25] By redox control of the self-assembled nanostructures, the catalytic activity for hydrolysis can be switched. The change of nanostructures self-assembled by seleno-compounds is mainly caused by the amphiphilicity transformation between the selenide and the selenoxide.[22–24] Stimulated by the switchable self-assembly of seleno-compounds, we planned to utilize this property combined with the catalytic function of Se to construct a smart GPx mimic with controllable activity through adjusting supramolecular morphology change by substrates (GSH and ROOH).

In order to achieve this goal, Fmoc-phenylalanine-derived selenide was designed and synthesized. The design presented herein consists of a standard amphiphilic motif (Scheme 1A): a hydrophobic tail, to which we assigned a Fmoc-phenylalanine and a hydrophilic head, 2,2′-selenodiethanol. We chose Fmoc-phenylalanine as hydrophobic tail because Fmoc-phenylalanine and its derivatives can readily self-assemble into various nanostructures[26–31] in aqueous solution through hydrogen bonding, hydrophobic interaction and π–π stacking. Moreover, such amino acid-based materials are commonly considered low-toxic and biocompatible, which are promising to be applied in organisms. The use of 2,2′-selenodiethanol as the hydrophilic head is under the consideration of the below factors. On one hand, if this molecule could self-assemble into nanostructures, at the reduction state (*i.e.* selenide), the hydrophobic Se as the catalytic center should be embedded into the internal, reducing the mimic to low or no activity (Scheme 1B). On the other hand, under the oxidation of ROOH, hydrophobic selenide turns into hydrophilic selenoxide, making Se expose on the surface of the nanostructure with high activity (Scheme 1B).

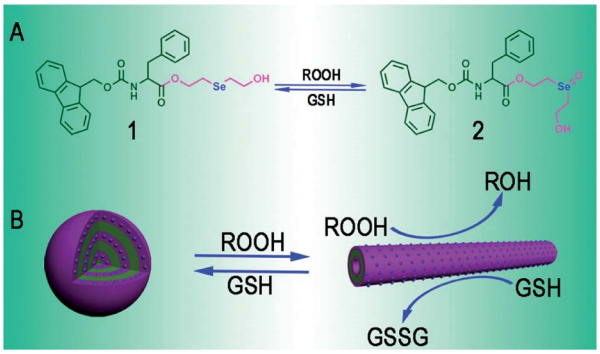

Scheme 1 (A) Molecular structures of the Se-containing compounds. (B) Schematic illustration of the redox control of GPx catalytic activity triggered by morphology transformation between NSs and NTs.

As expected, the Fmoc-phenylalanine-derived selenide can self-assemble into nanospheres with low GPx catalytic activity. Under the treatment of ROOH, selenide rapidly transforms into selenoxide. The tiny molecular structure variation directly causes the macroscopic morphology to change from nanospheres to nanotubes accompanied by significant increase in catalytic activity. The nanotubes can further switch into nanospheres under the reduction of GSH. The switchable property makes this material available as an efficient mimic to control the dynamic balance of ROOH through auto-sensing the substrates and then auto-changing its activity. The internal structures of the self-assemblies were characterized by AFM, SEM, TEM, CD and fluorescence spectra. The possible relationship between the catalytic activity and the structures is discussed.

Materials and methods

Materials

Fmoc-protected phenylalanine (Fmoc-Phe-OH) was purchased from GL Biochem (Shanghai) Ltd. and used as received. Dicyclohexylcarbodiimide (DCC) was obtained from Sinopharm Chemical Reagent Co. Ltd. and used directly. Selenium powder, sodium borohydride ($NaBH_4$) and 4-dimethylaminopyridine (DMAP) were obtained from Aladdin Industrial Corporation. Glutathione (GSH), glutathione reductase and β-nicotinamide adenine dinucleotide phosphate (NADPH) were purchased from Sigma. Tetrahydrofuran (THF) was rigorously dried with

sodium. Other solvents were of analytical grade and used without further purification. Water used was from a Millipore water purification system with a minimum resistivity of 18.0 MΩ cm.

Instruments and measurement

^{1}H NMR spectroscopy, ^{13}C NMR spectroscopy, ESI-MS spectrometric analyses and Fourier transform infrared (FT-IR) spectroscopy were used to characterize the molecular structures of the synthesized compounds. ^{1}H NMR spectra and ^{13}C NMR spectroscopy were recorded with a Bruker AVANCE III 500 apparatus using a tetramethylsilane (TMS) proton signal as the internal standard. ESI-MS spectrometric analyses were performed at the Thermo Finnigan LCQ AD System. FT-IR spectra were obtained using a Bruker Vector 22 FT-IR spectrometer at ambient temperature. Melting point (m. p.) measurement was obtained using an XT-4 Melting-point Apparatus with Microscope. Optical microscopy, atomic force microscopy (AFM), scanning electron microscopy (SEM), transmission electron microscopy (TEM), UV-vis spectroscopy, fluorescence emission spectroscopy and circular dichroism (CD) measurements were carried out to characterize the structural conformations and morphologies of NSs and NTs. AFM imaging was performed using a NanoScope Multi-Mode-AFM (Veeco, USA). SEM observations were obtained using a JEOL JSM-6700F scanning electron microscope with a primary electron energy of 3 kV. TEM measurements were obtained using a JEOL model JEM-3010 at 300 kV. All samples were stained by 2% phosphotungstic acid for 2 minutes. UV-vis spectra were monitored on a Shimadzu 3100 UV-vis-NIR spectrophotometer. Fluorescence emission spectra were recorded using a Perkin-Elmer LS-55 luminance spectrometer. CD spectra were obtained using a Jasco J-810 spectropolarimeter under a nitrogen atmosphere.

Synthesis and characterization of compound 1

2,2′-selenodiethanol (1.70 g, 10 mmol), DCC (1.03 g, 5 mmol) and DMAP (19 mg) were suspended in anhydrous THF (10 mL) under N_2, Fmoc-Phe-OH (1.95 g, 5 mmol) in 30 mL of anhydrous THF was added drop wise. The mixture was stirred overnight. After filtration, the solvent was evaporated under reduced pressure. The resulting crude product was purified by flash chromatography (10 : 1 dichloromethane–ethyl acetate) to give the product as a yellow solid, yield 47%. ^{1}H NMR (500 MHz, DMSO-d_6, 25 °C) δ (ppm): 2.66 (m, 4H), 2.93 (m, 1H), 3.06 (dd, 1H), 3.60 (m, 2H), 4.25 (m, 6H), 4.84 (t, 1H), 7.28 (m, 7H), 7.42 (t, 2H), 7.65 (t, 2H), 7.89 (m, 3H); ^{13}C NMR (500 MHz, DMSO-d_6, 25 °C) δ (ppm): 21.4, 27.1, 37.0, 47.1, 56.1, 62.0, 65.1, 66.2, 120.6, 125.7, 127.0, 127.5, 128.1, 128.7, 129.6, 137.9, 141.2, 144.2, 156.4, 172.2; $C_{28}H_{29}NO_5Se$ ESI-MS: calc. $[M + H]^+ = 540.1$, obsvd $[M + H]^+ = 540.1$; m. p.: 56.5 °C.

Synthesis and characterization of compound 2

To a solution of compound **1** in methanol, 2 equiv. of H_2O_2 was added. After stirring for 20 min, the reaction was completely accomplished (detected by thin layer chromatography (TLC)). The removal of solvent by vacuum equivalently yielded the product as a yellow solid, total yield 98%. ^{1}H NMR (500 MHz, DMSO-d_6, 25 °C) δ (ppm): 2.81 (m, 1H), 2.92 (m, 2H), 3.09 (m 4H) 3.82 (m, 2H), 4.24 (m, 4H), 4.46 (m, 2H), 5.14 (s, 1H), 7.27 (m, 8H), 7.42 (t, 2H), 7.65 (t, 2H), 7.89 (d, 2H); ^{13}C NMR (500 MHz, DMSO-d_6, 25 °C) δ (ppm): 36.9, 44.6, 47.0, 50.7, 55.3, 56.0, 59.1, 66.2, 120.6, 125.7, 127.0, 127.6, 128.1, 128.7, 130.0, 137.9, 141.2, 144.2, 156.4, 172.1; $C_{28}H_{29}NO_6Se$ ESI-MS: calc. $[M + H]^+ = 556.1$, obsvd $[M + H]^+ = 556.1$; m. p.: 34 °C.

Preparation of nanospheres (NSs)

Se-containing compound **1** was dissolved in methanol at a concentration of 50 mM. The self-assembled NSs were prepared by diluting the stock solution with ultrapure water to a final concentration of 1 mM.

Preparation of nanotubes (NTs)

The preparation process of NTs was the same as that of the NSs except that compound **1** was replaced by compound **2**.

Determination of the critical aggregation concentration (CAC)

To the aqueous solutions of compound **1** or **2** with different concentrations, 0.5 μM of fluorescein was added. After sonication for 10 min and then standing still overnight, the fluorescent emission spectra of the solutions were measured. The exciting wavelength is 490 nm. The CAC is indicated by the abrupt variation of the fluorescent intensity at 515 nm with the increasing concentration of **1** or **2**.

Determination of GPx catalytic activity

The GPx catalytic activity was monitored in a coupled reductase assay system using GSH and ROOH as substrates, according to the method reported by Wilson[32] (the following chemical equations).

$$2GSH + ROOH \xrightarrow{\text{Enzyme}} GSSG + ROH + H_2O \quad (1)$$

$$GSSG + NADPH + H^+ \xrightarrow{\text{Glutathione reductase}} 2GSH + NADP^+ \quad (2)$$

The reaction was carried out at 37 °C in 500 μL of phosphate buffer (pH = 7.0, 50 mM) containing 1 mM EDTA, 1 mM GSH, 1 unit of glutathione reductase and 0.2 mM GPx mimic. After preincubation for 5 min, 0.25 mM NADPH was added. The mixture was incubated for another 3 min. Then, the reaction was initiated by the addition of 0.25 mM cumene hydroperoxide (CUOOH) or H_2O_2. Considering the UV spectrum of NADPH, which exhibits a strong absorption peak at 340 nm, the initial rates for the reduction of ROOH by GSH were determined by monitoring the decrease of NADPH absorption at 340 nm with a Shimadzu 2450 UV-vis-NIR spectrophotometer. The appropriate control activity without GPx mimics was also assayed and subtracted from the catalytic reactions.

Results and discussion

Reversible conversion between selenide 1 and selenoxide 2

The feasibility of reversible conversion between selenide and selenoxide has been proved previously. In this system, the molecular structures of the amphiphilic Se-containing compounds **1** and **2** are shown in Scheme 1. Experimentally, the addition of 2 equiv. of H_2O_2 or CUOOH to the methanol solution of **1** quickly produced **2**, which could rapidly transform back to **1** upon the addition of 2 equiv. of GSH. TLC analyses indicated that both the oxidation and the reduction reaction achieved complete conversion and hardly generated by-products (Fig. S11†). ^{1}H NMR spectra, ^{13}C NMR spectra and ESI-MS confirmed the molecular structures of **1** and **2** (Fig. S2–S4 and S6–S8†). In TLC pictures, the difference in Rfs between **1** and **2** (Fig. S11A†) was indicative of the dissimilarity in the amphipathic property between the oxidized and reduced forms. The fact that **1** moved further than **2** demonstrated that the selenoxide is more hydrophilic than the selenide. Similar phenomena were also described in previous studies.

Characterization of the self-assembled nanostructures

To investigate the self-assembly behavior of compounds **1** and **2**, the CACs of **1** and **2** were first measured using a fluorescent probe method. The CAC of compound **1** is 0.018 mM, whereas of compound **2** is 0.055 mM (Fig. S10†). Both **1** and **2** can self-assemble into regular supramolecular nanostructures in water when the concentration is above the CAC. AFM, SEM and TEM tests were done to investigate the nanostructures of the self-assemblies. For compound **1**, as shown in Fig. 1A, the selenide could self-assemble into nanospheres (NSs) at 1 mM with a size ranging from 30–80 nm. In the case of compound **2**, the tiny molecular structure change from selenide to selenoxide directed great change in morphology. As shown in Fig. 1B, the self-assembly of compound **2** formed uniform and high aspect ratio fibrillar nanostructure with a diameter about several dozens of nanometers. Height AFM image revealed that the width of the self-assembly was about 12.6 nm (Fig. S12†). The fibrillar nanostructure tended to intertwine into larger bundles, which were visible under optical microscopy (Fig. S14†). To clearly look into the internal structure of the self-assembly, high resolution TEM micrographs were performed. HR-TEM images clearly revealed that the fibrillar nanostructures were nanotubes with dark hollows and relatively off-white walls (Fig. S13†). The well-defined nanotubes had a uniform external diameter of 12.5 nm, inner diameter of 4.5 nm and length of several dozens of micrometers, which was consistent with the observation of AFM. Dynamic light scattering (DLS) was further utilized to investigate the aggregation behaviors of **1** and **2** in aqueous solution. The DLS results (>100 nm) revealed that both **1** and **2** could form nanoscale structures in aqueous solution.

Morphological conversion between the NSs and the NTs

The redox triggered morphological change can be used as a powerful tool to adjust the self-assembly of the Se-containing compounds. Although the compound **1** and **2** can readily interconvert in organic media upon addition of redox reagents, once they self-assemble into NSs or NTs in aqueous solution, the conversion may not be so easy. UV-vis spectra were conducted to give a visualized observation of the conversion. As the molar extinction coefficients of NSs and NTs are different at 260 nm, the conversion ratio can be reflected by comparing the change in UV-vis spectra. As shown in Fig. 2, at concentration of 0.1 mM, a strong absorption of the NTs at about 260 nm could be observed. After the addition of 2 equiv. of GSH and stirring for 20 min, the peak at 260 nm greatly dropped, indicating the structure transition from NTs to NSs can be rapidly and effectively accomplished. When treating this solution with 1 equiv. of CUOOH for 20 min, a recovery of the absorbance could be clearly monitored, implying the reversion of the NTs. However, when CUOOH was replaced by H_2O_2, there was a slight increase at 260 nm. Even prolonging the reaction time to 2 hours, no evident change occurred. This declared that the structural

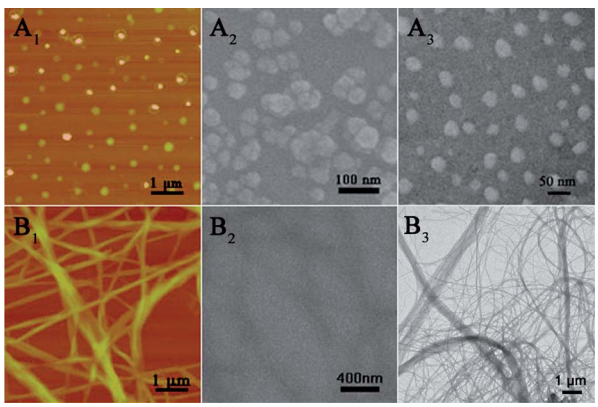

Fig. 1 Electron microscopic images of the self-assembled nanostructures. A1, A2 and A3 are AFM, SEM and TEM images of the NSs self-assembled from compound **1**, respectively; B1, B2 and B3 are AFM, SEM and TEM images of the NTs self-assembled from compound **2**, respectively.

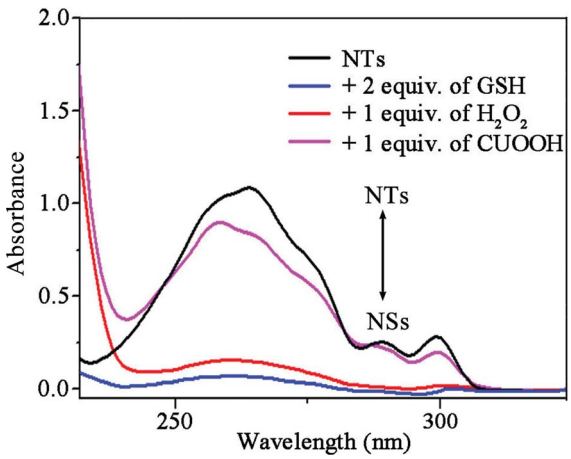

Fig. 2 UV-vis absorption spectra of the NTs (black) under the reduction of GSH (blue) and then oxidation of H_2O_2 (red) or CUOOH (pink).

transition from NSs to NTs triggered by H_2O_2 is more difficult than that by CUOOH. The redox switched self-assembly behaviours were further confirmed by optical microscopy and AFM. As shown in Fig. S15 and S16,† the addition of 2 equiv. GSH to the NTs rapidly yielded the NSs, which could convert back to NTs by the oxidation of 1 equiv. of CUOOH. Moreover, the tubular structure did not appear by the treatment of 1 equiv. of H_2O_2, which was consistent with the result of the UV-vis spectra. Only by addition of large excessive H_2O_2, the NTs could return. All these strongly demonstrated that the Se-containing compounds show an expected redox-switched self-assembly property.

Catalytic behaviours of the NSs and the NTs

The scavenging rate of ROOH can be evaluated by the GPx catalytic activity. The higher GPx activity suggests the more rapid scavenging rate of ROOH. For keeping the ROOH in a dynamic balance to maintain its beneficial physiological function and eliminate their harmful oxidative damage, a reasonable GPx mimic should behave as follows: when ROOH are abundant, it should exhibit high activity, whereas ROOH are reduced, it should exhibit low or no activity. As for this system, because the mimic appears to be a nanotube structure under the oxidation of ROOH, whereas a nanosphere structure under the reduction of GSH, the ideal result is that the NTs exhibit relatively high activity while the NSs are of no or low activity.

A coupled reductase assay system using GSH and ROOH (CUOOH or H_2O_2) as substrates was arrayed to monitor the GPx catalytic activity. The initial reaction rate was measured according to the decreased absorption value of the NADPH at 340 nm. The matched blank experiments without enzymatic mimics were also carried out. In the case of CUOOH as substrate, as expected, the initial reaction rate under the catalysis of NSs showed just a little increase compared with that without enzyme, indicated by a slight enhancement in the slope of the blue curve (Fig. 3A). Under identical conditions, the replacement of NSs with NTs presented a distinct slope increase compared with that of the NSs, indicating the remarkable increase in catalytic activity (see Table S1†). This demonstrated that the catalytic activities are closely associated with the structures of the enzymes. When H_2O_2 was employed as the substrate instead of CUOOH, a similar result was obtained (Fig. 3B). It is notable that in the case of H_2O_2, no catalytic activity can be detected under the catalysis of NSs. This is different from that of CUOOH. Although the activity is extremely low, it can be detected in the case of CUOOH. We attribute the possible reason to that the CUOOH oxidizes part of NSs to NTs, because NSs more easily switch to NTs in the presence of CUOOH instead of H_2O_2. These discoveries, such as the relatively high GPx activity of the NTs and extremely low or no activity of the NSs, verify the feasibility of our idea.

The secondary structures of the NSs and the NTs

Circular dichroism (CD) spectroscopy was employed to study the molecular orientations of the NSs and NTs. As shown in Fig. 4, the peaks at about 234 nm and 217 nm (the n–π*

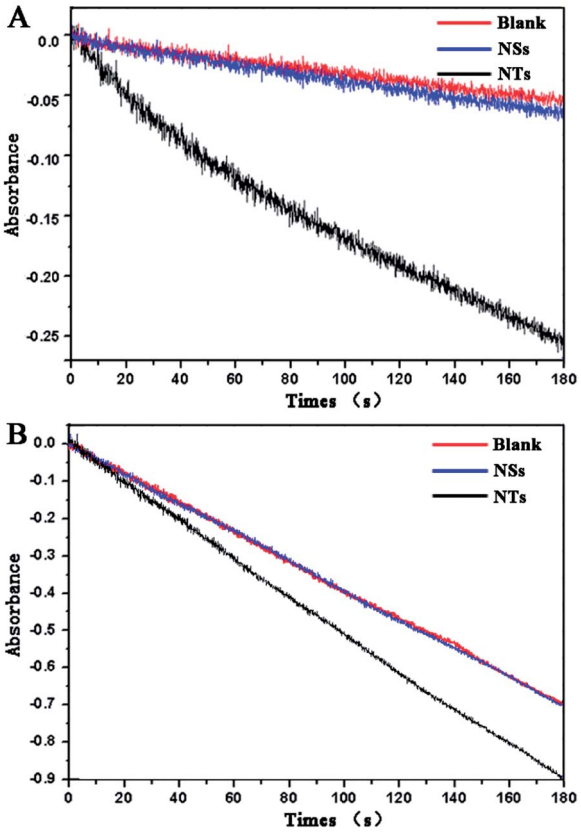

Fig. 3 Plots of absorbance *versus* time during the catalytic reduction of (A) CUOOH or (B) H_2O_2 using GSH as reducing substrate.

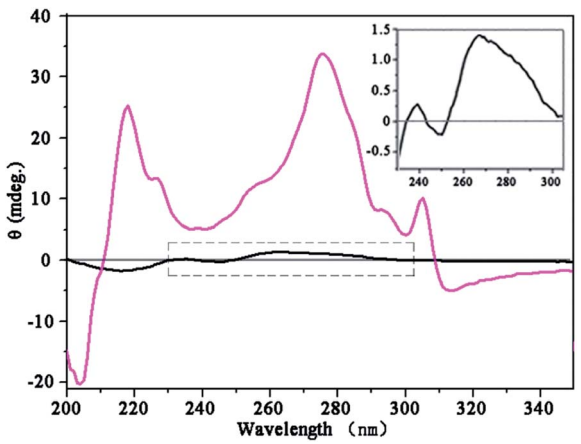

Fig. 4 Circular dichroism spectra of the NSs (black curve) and NTs (pink curve) at concentration of 1 mM.

transition) were detected in NSs and NTs, which indicated the superhelical arrangements of the amino acid residues of compound **1** and **2**.[26,33–35] The superhelical arrangements further induce the helical orientation of the fluorenyl groups, which was demonstrated by the cotton effects at 240–310 nm in the CD spectra.

In order to acquire more useful information on the self-assembly mechanism, fluorescence emission spectroscopy was

used to help evaluate the internal arrangement among the fluorenyl (Fmoc) moieties of **1** and **2**. In the case of compound **1**, at a low concentration of 0.01 mM, the NSs exhibited a maximum emission peak centered at 304 nm (Fig. 5). As the concentration increased to 10 mM, the maximum emission peak gradually shifted to 316 nm. The small red-shift from 304 to 316 nm was possibly due to the presence of fluorenyl excimer species, which were caused by the aggregation of the Fmoc groups during the self-assembly of **1**.[26,36,37] This red-shift also indicated an anti-parallel manner of fluorenyl rings (Fig. 6), which was supported by the shoulder at 365 nm.[33,38,39] In the emission spectrum, the observation of a small feature at 469 nm implied a small amount of J-aggregate of phenyl rings as well as fluorenyl rings.[38] In the case of compound **2**, similar results as compound **1** could be obtained. By increasing the concentration from 0.001 mM to 5 mM, the anti-parallel stacking of the Fmoc groups-induced red-shift (from 303 nm to 328 nm) could be observed, which suggested that compound **2** was gradually transforming from the monomeric form to the well-defined NTs. The emergence of the small feather at 467 nm implied that multiple fluorenyl groups aggregate *via* π–π stacking. Combining the information from CD and fluorescence spectra indicates that the π–π stacking among the Fmoc groups can provide effective driving forces and great possibility for the self-assembly of Fmoc-protected amino acid derivatives, and the Fmoc-phenylalanine-based building blocks are mainly arrayed in an anti-parallel manner. That is one of the reasons why we chose this type of molecules as the building blocks.

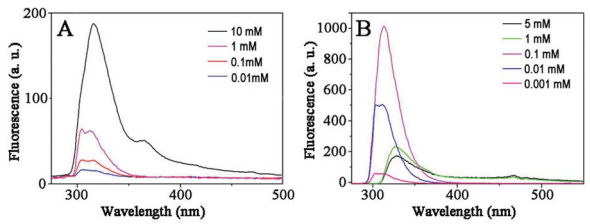

Fig. 5 Fluorescence emission spectra of (A) NSs and (B) NTs at different concentrations.

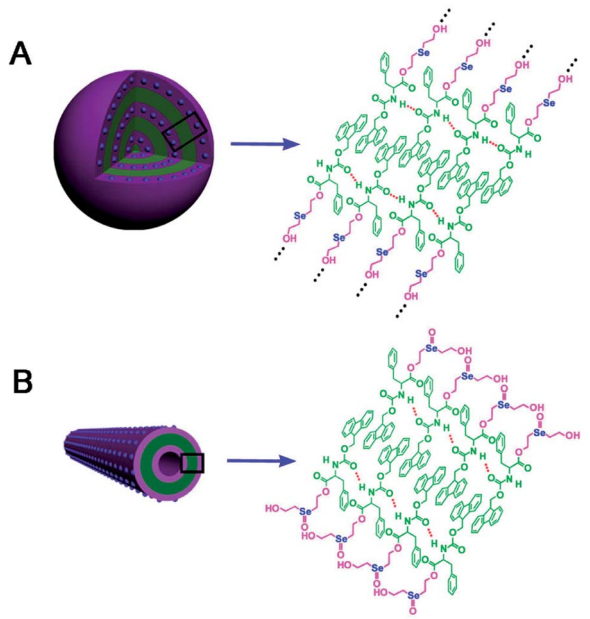

Fig. 6 The possible modes of the self-assembly from (A) compound **1** and (B) compound **2**.

The relationship between the GPx activity and the self-assembled nanostructures

On account that the arrangement pattern of the NSs and NTs mainly adopts anti-parallel manner and the strong intermolecular hydrogen bond generally exists among the aggregates self-assembled by the amino acid derivatives, the configurations of compounds **1** and **2** are probably in a completely extended mode. Assuming all the bonds among the main chain are carbon–carbon bonds, these two seleno-compounds containing 17 carbons in the main chain would have a length of about 2.2 nm.[40] Thus, a bilayer is about 4 nm, which is simply corresponding to the thickness of the nanotube walls (Fig. 6B). This suggests that the NTs are made up of a single bilayer of the compound **2**. As for the NSs, the average diameter of 50 nm implies that there are on average 6 bilayers in the sphere structure. The difference in bilayer number of the nanostructures between the NTs and the NSs may be an important reason to explain their significant activity variation. In the case of NSs, the multi-layer structure makes the catalytic selenium covered into the interior of the NSs (Fig. 6A), which makes it unable to contact the substrates, resulting in extremely low activity, whereas for the NTs, the single layer structure enables the selenium to expose onto the surface of the nanostructure, thus it can effectively contact the substrate and quickly catalyze the reaction.

Conclusions

In summary, a novel GPx mimic with tunable activity through mediating the structure of self-assembly was successfully fabricated. By redox control of the reversible switch of the microscopic molecular structure and amphiphilicity of the Se-containing compounds to achieve macroscopical morphology transition, the catalytic Se could be buried into the hydrophobic interior and exposed to the surface of the nanostructures reversibly, resulting in switchable GPx catalytic activity. More importantly, the mimic exhibits high activity to quickly scavenge ROOH when the system is under an oxidation environment and shows low activity when under a reduction condition, which makes it possible to maintain the ROOH in an appropriate amount to maintain the salutary function and avoid their harmful side effect. This endows it with both an excellent sensor function to auto-detect the signal of ROOH and a smart enzymatic effect to controllably clear out ROOH through redox-induced morphological change. Although the absolute GPx activity is not so high compared with that of natural GPxs or other GPx mimics, the dual functions of a sensor and an enzyme make this smart GPx mimic provide a novel strategy for

generating supramolecular artificial enzymes with multi-properties and open a new method to investigate the relationship between the structure and catalytic activity of the enzymes.

Acknowledgements

We are grateful of the financial support from the Natural Science Foundation of China (21234004, 91027023, 21274051, 21221063, 21004028), the 111 project (B06009), and the Chang Jiang Scholars Program of China.

Notes and references

1 H. Sies, *Exp. Physiol.*, 1997, **82**, 291–295.
2 H. Sies, *Angew. Chem., Int. Ed. Engl.*, 1986, **25**, 1058–1071.
3 H. Sies, Oxidative Stress: Introductory Remarks, in *Oxi-dative Stress*, ed. H. Sies, Academic Press, London, 1985, p. 1.
4 L. Flohé, G. Loschen, W. A. Günzler and E. Eichele, *Hoppe-Seyler's Z. Physiol. Chem.*, 1972, **353**, 987–999.
5 T. C. Stadtman, *J. Biol. Chem.*, 1991, **266**, 16257–16260.
6 O. Epp, R. Ladenstein and A. Wendel, *Eur. J. Biochem.*, 1983, **13**, 51–69.
7 T. Kanda, L. Engman, I. A. Cotgreave and G. Powis, *J. Org. Chem.*, 1999, **64**, 8161–8169.
8 C. Jacob, G. E. Arteel, T. Kanda, L. Engman and H. Sies, *Chem. Res. Toxicol.*, 2000, **13**, 3–9.
9 A. L. Braga, E. E. Alberto, L. C. Soares, J. B. T. Rocha, J. H. Sudati and D. H. Roos, *Org. Biomol. Chem.*, 2009, **7**, 43–45.
10 K. P. Bhabak and G. Mugesh, *Chem.–Asian J.*, 2009, **4**, 974–983.
11 C. P. Prabhu, P. P. Phadnis, A. P. Wadawale, K. I. Priyadarsini and V. K. Jain, *J. Organomet. Chem.*, 2012, **713**, 42–50.
12 M. McNaughton, L. Engman, A. Birmingham, G. Powis and I. A. Cotgreave, *J. Med. Chem.*, 2004, **47**, 233–239.
13 J. Q. Liu, G. M. Luo, X. J. Ren, Y. Mu, Y. Bai and J. C. Shen, *Biochim. Biophys. Acta*, 2000, **1481**, 222–228.
14 G. M. Luo, Z. Q. Zhu, L. Ding, G. Gao, Q. A. Sun, Z. Liu, T. S. Yang and J. C. Shen, *Biochem. Biophys. Res. Commun.*, 1994, **198**, 1240–1247.
15 X. M. Liu, L. A. Silks, C. P. Liu, M. Ollivault-Shiflett, X. Huang, J. Li, G. M. Luo, Y. M. Hou, J. Q. Liu and J. C. Shen, *Angew. Chem., Int. Ed.*, 2009, **121**, 2054–2057.
16 C. X. Hou, Q. Luo, J. Q. Liu, L. Miao, C. Q. Zhang, Y. Z. Gao, X. Y. Zhang, J. Y. Xu, Z. Y. Dong and J. Q. Liu, *ACS Nano*, 2012, **6**, 8692–8701.
17 S. J. Yu, Y. Z. Yin, J. Y. Zhu, X. Huang, Q. Luo, J. Y. Xu, J. C. Shen and J. Q. Liu, *Soft Matter*, 2010, **6**, 5342–5350.
18 Y. Tang, L. P. Zhou, J. X. Li, Q. Luo, X. Huang, P. Wu, Y. G. Wang, J. Y. Xu, J. C. Shen and J. Q. Liu, *Angew. Chem., Int. Ed.*, 2010, **49**, 3920–3924.
19 X. Huang, Y. Z. Yin, Y. Tang, X. L. Bai, Z. M. Zhang, J. Y. Xu, J. Q. Liu and J. C. Shen, *Soft Matter*, 2009, **5**, 1905–1911.
20 X. Huang, Y. Z. Yin, X. Jiang, Y. Tang, J. Y. Xu, J. Q. Liu and J. C. Shen, *Macromol. Biosci.*, 2009, **9**, 1202–1210.
21 L. Wang, H. X. Zou, Z. Y. Dong, L. P. Zhou, J. X. Li, Q. Luo, J. Y. Zhu, J. Y. Xu and J. Q. Liu, *Langmuir*, 2014, **30**, 4013–4018.
22 H. F. Ren, Y. T. Wu, N. Ma, H. P. Xu and X. Zhang, *Soft Matter*, 2012, **8**, 1460–1466.
23 Y. Ding, Y. Yi, H. P. Xu, Z. Q. Wang and X. Zhang, *Chem. Commun.*, 2014, **50**, 2585–2588.
24 H. P. Xu, W. Cao and X. Zhang, *Acc. Chem. Res.*, 2013, **46**, 1647–1658.
25 X. M. Miao, W. Cao, W. T. Zheng, J. Y. Wang, X. L. Zhang, J. Gao, C. B. Yang, D. L. Kong, H. P. Xu, L. Wang and Z. M. Yang, *Angew. Chem., Int. Ed.*, 2013, **52**, 7781–7785.
26 A. M. Smith, R. J. Williams, C. Tang, P. Coppo, R. F. Collins, M. L. Turner, A. Saiani and R. V. Ulijn, *Adv. Mater.*, 2008, **20**, 37–41.
27 Z. M. Yang and B. Xu, *Chem. Commun.*, 2004, 2424–2425.
28 J. Gao, H. M. Wang, L. Wang, J. Y. Wang, D. L. Kong and Z. M. Yang, *J. Am. Chem. Soc.*, 2009, **131**, 11286–11287.
29 Z. M. Yang, H. W. Gu, Y. Zhang, L. Wang and B. Xu, *Chem. Commun.*, 2004, 208–209.
30 P. D. Thornton, R. J. Mart, S. J. Webb and R. V. Ulijn, *Soft Matter*, 2008, **4**, 821–827.
31 A. K. Das, R. Collins and R. V. Ulijn, *Small*, 2008, **4**, 279–287.
32 S. R. Wilson, P. A. Zucker, R. R. C. Huang and A. Spector, *J. Am. Chem. Soc.*, 1989, **111**, 5936–5939.
33 Z. M. Yang, H. W. Gu, D. G. Fu, P. Gao, J. K. Lam and B. Xu, *Adv. Mater.*, 2004, **16**, 1440–1443.
34 *Circular Dichroism: Principles and Applications*, ed. N. Berova, K. Nakanishi and R. W. Woody, Wiley-VCH, Weinheim, Germany, 2nd edn, 2000, ch. 21.
35 Y. Zhang, H. W. Gu, Z. M. Yang and B. Xu, *J. Am. Chem. Soc.*, 2003, **125**, 13680–13681.
36 O. Carny, D. E. Shalev and E. Gazit, *Nano Lett.*, 2006, **8**, 1594–1597.
37 R. Djalali, Y. Chen and H. Matsui, *J. Am. Chem. Soc.*, 2002, **124**, 13660–13661.
38 R. V. Ulijn, *J. Mater. Chem.*, 2006, **16**, 2217–2225.
39 D. Schweitzer, K. H. Hausser and M. W. Haenel, *Chem. Phys.*, 1978, **29**, 181–185.
40 H. C. Fry, M. G. Jamie, M. J. Medina, U. M. Ricoy, D. J. Gosztola, M. P. Nikiforov, L. C. Palmer and S. I. Stupp, *J. Am. Chem. Soc.*, 2012, **134**, 14646–14649.